A Parabolised Stability Equation based Broadband Shock-Associated Noise Model

Marcus H Wong, Daniel Edgington-Mitchell, Damon Honnery, André Cavalieri, Peter Jordan

A Parabolised Stability Equation based Broadband Shock-Associated Noise Model

Marcus H. Wong*, Daniel Edgington-Mitchell† and Damon Honnery ‡
Laboratory for Turbulence Research in Aerospace and Combustion (LTRAC), Department of Mechanical and Aerospace Engineering, Monash University, Melbourne, VIC 3800, Australia

André V. G. Cavalieri §
Instituto Tecnológico de Aeronáutica, São José dos Campos, SP, 12228-900, Brazil

Peter Jordan¶
Institut PPrime CNRS - Université de Poitiers - ENSMA, Poitiers, 86036, France

Wavepacket models have been used extensively to predict the noise produced from turbulent subsonic and supersonic jets. Such wavepackets, which represent the organised structures of the flow, are solutions to the linearised Navier-Stokes equations. Using a kinematic two-point model, Wong et al. [1] have indicated the importance of incorporating coherence decay in modelling broadband shock-associated noise (BBSAN) in supersonic jets. In this work, we aim to improve the model by using solutions from linear parabolised stability equations (PSE) to model the wavepacket part of the BBSAN source. The two-point coherence of the wavepackets is obtained from large-eddy simulation (LES) data of a $M_j = 1.5$ fully-expanded isothermal supersonic jet [2]. The aim is to build a dynamic sound-source model for BBSAN that would improve on the simplified line-source model proposed by Wong et al. [3]. We find that a frequency dependent coherence decay length scale is important in order to suppress the higher-order harmonic peaks [4] and to obtain the correct BBSAN peak shape. Moderate agreement up to $St = 1$ was found between the current noise predictions and those from experimental data.

I. Nomenclature

ω	=	wavepacket frequency
θ	=	azimuthal co-ordinate
c_{s_n}	=	amplitude coefficient of the shock cells
G	=	Green's function
k_s	=	shock-cell wavenumber
k_h	=	hydrodynamic wavenumber
L	=	longitudinal extent of wavepacket
L_c	=	coherence length of wavepacket
m	=	azimuthal mode number
M_j	=	ideally-expanded Mach number
r	=	radial co-ordinate
u_s	=	shock cell velocity fluctuation
u_t	=	wavepacket fluctuations
$\hat{u}^*_\omega$	=	velocity fluctuations at a frequency ω
x	=	axial co-ordinate

*PhD Student, Laboratory for Turbulence Research in Aerospace and Combustion (LTRAC), Department of Mechanical and Aerospace Engineering, Monash University, Melbourne, VIC 3800, Australia

†Senior Lecturer, Laboratory for Turbulence Research in Aerospace and Combustion (LTRAC), Department of Mechanical and Aerospace Engineering, Monash University, Melbourne, VIC 3800, Australia

‡Professor, Laboratory for Turbulence Research in Aerospace and Combustion (LTRAC), Department of Mechanical and Aerospace Engineering, Monash University, Melbourne, VIC 3800, Australia

§Assistant Professor, Divisão de Engenharia Aeronáutica, Instituto Tecnológico de Aeronáutica

¶Research-Scientist, Institute PPrime, CNRS - Université de Poitiers - ENSMA, UPR 3346, 43 Rue de l'Aérodrome, 86036 Poitiers, France

II. Introduction

Broadband shock-associated noise (BBSAN) in supersonic jets is generated when there is a 'mismatch' in pressure between the exiting jet flow and the ambient conditions. While other types of noise exist such as mixing noise [5] and screech [6, 7], BBSAN remains important for many modern aircraft [8]. The generation of noise is due to the weak interaction of shock-cells with the downstream-convecting turbulent structures of the jet. The study and modelling of BBSAN has been well documented in literature [9–13]. A review of supersonic jet noise is provided by Tam [14]. Although progress has been made in understanding this form of jet noise, a reduced-order model that links the radiated sound field to the acoustically important part of the flow field over a broad frequency range remains elusive.

BBSAN is characterised by a broad, high frequency peak that is dependent on observer location. The most intense noise is towards the sideline and upstream directions. As the observer location moves downstream, the broad peak shifts to higher frequencies and the spectral peak width increases. This directional dependence of the peak frequency f_p is predicted by

$$f_p = \frac{U_c}{L(1 - M_c cos(\theta))}, \tag{1}$$

where U_c is the convection velocity, L is the shock-cell spacing, M_c is the convection Mach number and θ is the observer angle measured from the downstream jet axis.

As proposed by Lele [15], the non-linear acoustic source (S) for BBSAN in terms of frequency is modelled by the interaction between fluctuations due to turbulence (u_t) and modulations due to the quasi-periodic shock-cells (u_s)

$$S(\mathbf{x}, \omega) = u_s(\mathbf{x}) \times u_t(\mathbf{x}, \omega). \tag{2}$$

To obtain the sound pressure field, the acoustic source term can be propagated using Lighthill's [16] acoustic analogy

$$\frac{\partial^2 \rho'}{\partial t^2} - c_\infty^2 \bigtriangledown^2 \rho' = \frac{\partial^2}{\partial x_i x_j} S, \tag{3}$$

where ρ' is the fluctuating density, c_∞^2 is the far-field speed of sound and S is the source term. The double spatial derivative can be passed onto the Green's function [17]. The source term, which encapsulates the non-linearities of the flow, drives the fluctuations in the far-field. The utilisation of the acoustic analogy to predict BBSAN has also been performed by Kalyan and Karabasov [12], Morris and Miller [18] amongst others. The far-field pressure can be obtained analytically using a free-field Green's function

$$p(\mathbf{x}, \omega) = \frac{1}{4\pi} \int S(\mathbf{x}, \omega) e^{\mathrm{i}|\mathbf{x}-\mathbf{y}|} \frac{dV}{|\mathbf{x} - \mathbf{y}|}. \tag{4}$$

Recently, wavepacket models have been proposed in the modelling of subsonic jet noise [19, 20]. Pioneered by the seminal findings of Mollo-Christensen [21] and Crow and Champagne [22], wavepacket descriptions provide a direct link between the instabilities of the flow with the radiated sound field. Wavepackets, or instability waves, represent the coherent structures of a turbulent flow; they grow from the initial instabilities near the nozzle exit, become neutrally stable some distance downstream and then decay. The signature of wavepackets, which can be obtained via azimuthal decomposition of the turbulent jet [23], shows these to have different length scales compared to the energy-containing eddies [24]. For a given frequency, their non-compact shapes can also be clearly seen in the leading spectral proper orthogonal decomposition (SPOD) modes[25]. The non-compact nature of the resulting convected wave gives rise to the distinctive directivity of jet noise [26]. The detection of wavepackets has been supported by numerous near-field pressure measurement studies [27–30]. Their results are further supported in the comparisons made between velocity fields and stability calculations by Cavalieri et al. [31] and recent resolvent analysis studies by Schmidt et al. [25], Lesshafft et al. [32]. Sasaki et al. [33] have also found that the evolution of the lower-order azimuthal modes can be predicted using linear wavepackets up to a Strouhal value of $St = 4$. More recently, wavepacket models have also been developed and applied to non free-field cases such as jets in the vicinity of a flat plate [34].

While linear wavepacket models have been successful in modelling the large-scale structures in subsonic turbulent jets, the predicted sound pressure level is several orders of magnitude less than those obtained from experiments [35–37].

The aforementioned shortcomings can be resolved when we include wavepacket 'jitter' [38]; the desynchronisation of wavepackets due to the action of background turbulence [35, 36, 39]. Using two-point statistics of a turbulent jet, the jittering behaviour is represented as coherence decay. The decay of coherence can be seen in both numerical and experimental PIV data [24]. The two-point coherence function γ^2, extracted from the magnitude square coherence (MSC) of axial velocity between points x_1 and x_2, can be modelled using a simple Gaussian function

$$\gamma^2(x_1, x_2, \omega) = \exp\left(-2\frac{(x_1 - x_2)^2}{L_c^2(\omega)}\right), \tag{5}$$

where $L_c(\omega)$ is given as the characteristic length scale for coherence decay. Cavalieri and Agarwal [35] found that for a given sound source, the average amplitude, phase and also its coherence function γ^2 need to be modelled correctly to match the original source. Hence, for a given frequency ω, the power spectral density of the far-field sound $\langle p(\boldsymbol{r}, \omega)p^*(\boldsymbol{r}, \omega)\rangle$ at an observer location position $\boldsymbol{r}$ can now be obtained using the following expression

$$\langle p(\boldsymbol{r}, \omega)p^*(\boldsymbol{r}, \omega)\rangle \approx \int_V \int_V \langle \tilde{S}(x_1, \omega)\tilde{S}^*(x_2, \omega)\gamma(x_1, x_2, \omega)\rangle G(\boldsymbol{r}, x_1, \omega)G^*(\boldsymbol{r}, x_2, \omega)dx_1 dx_2. \tag{6}$$

The linear two-point description of the source $S(x_1, \omega)S^*(x_2, \omega)$ is multiplied by the coherence decay term $\gamma(x_1, x_2, \omega)$ to form the full cross-spectral density (CSD) $\tilde{S}(x_1, \omega)\tilde{S}^*(x_2, \omega)$ of the original source found in the integral of equation 6. The relationship between the linear and full statistical source is given as

$$\tilde{S}(x_1, \omega)\tilde{S}^*(x_2, \omega) = S(x_1, \omega)S^*(x_2, \omega)\gamma(x_1, x_2, \omega). \tag{7}$$

Instability wave models have also been used in perfectly-expanded [40] and imperfectly-expanded supersonic flows [10, 15, 41, 42]. In perfectly-expanded flows characterised by supersonic convection velocity, the results of Sinha et al. [40] show that coherence decay is here less important to obtain the sound radiation at peak polar angles due to the phase speeds of the wavepackets being supersonic and thus capable of radiating to the far-field efficiently. To study the influence of coherence decay in shock-containing flows, Wong et al. [1] used a line-source wavepacket model containing only the $m = 0$ axisymmetric mode. It was found that coherence decay, rather than increasing acoustic efficiency as in the subsonic case, suppressed artificial higher-order harmonic peaks when additional shock-cell modes are included. The peaks occur due to the higher order shock-cell modes interacting with the instability waves of the mean flow. These spurious peaks were also previously predicted by both Tam et al. [10] and Lele [15]; both these models have perfectly-coherent sources. Using the source description in equation 2, the CSD for BBSAN found in equation 6 is now modelled as a two-point line source [1] expressed as

$$\begin{aligned}\tilde{S}(x_1, \omega)\tilde{S}^*(x_2, \omega) \quad = \quad & A^2(\omega)e^{-\left(\frac{x_1 - x_0}{L(\omega)}\right)^2} e^{-\left(\frac{x_2 - x_0}{L(\omega)}\right)^2} \left\{e^{\mathrm{i}k_h(\omega)(x_1 - x_2)}\right\} e^{\left(-\frac{(x_1 - x_2)^2}{L_c^2(\omega)}\right)} \times \\ & \sum_{n_1} c_{s_{n_1}} \left\{e^{\mathrm{i}k_{s_{n_1}}x_1} + e^{-\mathrm{i}k_{s_{n_1}}x_1}\right\} \sum_{n_2} c_{s_{n_2}} \left\{e^{\mathrm{i}k_{s_{n_2}}x_2} + e^{-\mathrm{i}k_{s_{n_2}}x_2}\right\},\end{aligned} \tag{8}$$

where a wavepacket at a given frequency is characterised by its hydrodynamic wavenumber k_h and two length scales L and L_c, which are the wavepacket amplitude envelope and coherence lengths respectively. The shock-cell component is modelled using the Pack & Prandtl model, where k_{s_n} and c_{s_n} are the wavelength and amplitude of the n^{th} shock-cell mode respectively. Wong et al. [3] found that the inclusion of coherence decay, while able to suppress higher-order peaks, led to poor agreement at frequencies lower than the peak frequency. It was assumed that this was due to the use of ad-hoc constant values of k_h, L and L_c. Moreover, the 1D line source assumption may be overly restrictive due to the distributed nature of the acoustic sources for BBSAN [42, 43]. In order to assess these issues, a more realistic representation of the wavepacket parameters as a function of frequency is necessary.

The current work aims to extend the model proposed by Wong et al. [1], by obtaining a volumetric description of u_t from stability theory and large-eddy simulation (LES) data. In order to develop a more realistic two-point model and to establish a link to linear stability theory, the axisymmetric part of the turbulent fluctuations are approximated via solutions to the parabolised stability equations (hereinafter PSE). The modulations due to the shocks u_s are obtained from the Pack & Prandtl model [44, 45]. The methodology is similar to Ray and Lele [42] who used PSE solutions coupled with shock-cell solutions, but differs in so far we incorporate two-point coherence in the source model. The

mean flow used for the PSE analysis will be extracted from the LES data of Brès et al. [2]. To compare with the original line source model (equation 8), both the u_s and u_t fluctuations are integrated radially [39]. The two-point coherence behaviour is extracted from the MSC of the decomposed streamwise velocity originating from the same LES data set. The BBSAN predictions are compared to experimental data [18] and the analytical wavepacket BBSAN model of Wong et al. [1].

The paper is organised as follows. The LES dataset of Brès et al. [2] is briefly discussed in section III. In section IV we present the proposed methodology to model BBSAN and the construction of the source terms. Emphasis is placed on the approach used to solve the linear PSE and the extraction of coherence information from the LES data. In section V we present preliminary results from the PSE and compare them to LES data in section VI. Results for coherence decay length scales are shown in section VII and the resulting far-field BBSAN predictions are presented in section VIII.

III. LES Database

A large-eddy simulation database of a $M_j = 1.5$ supersonic ideally-expanded isothermal jet is used in this present study. The simulation was performed using the compressible flow solver "Charles" developed at Cascade Technologies [2], on an unstructured adapted grid with 40 million cells. This database is an extension of the previous work by Brès et al. [46], with the flow conditions and nozzle geometry (convergent-diverging) matching those of the experiment carried out at the United Technologies Research Center (UTRC) anechoic jet facility [47]. The main differences with the previous simulations are that wall modelling and near-wall adaptive mesh refinement are now employed on the internal nozzle surface, and that the simulated Reynolds number is now $Re = \rho_j U_j D/\mu_j = 1.78 \times 10^6$, matching the experimental value. This is done to better capture/model the state of the boundary layer inside the nozzle, which has been shown to be important for flow field and noise predictions [48]. This modelling leads to (nominally) turbulent boundary layer profiles at the nozzle exit. The rest of the numerical setup is identical to Brès et al. [2]. A slow co-flow of $M_{co} = 0.1$ is also included in the simulation to match the experimental conditions. The nozzle exit is centered at $(x, y, z) = (0, 0, 0)$ and the axisymmetric computation domain extends to $45D$ and $20D$ in the streamwise and radial direction respectively. To facilitate post-processing and analysis, the LES data is interpolated from the original unstructured LES grid onto a structured cylindrical grid with uniform spacing in azimuth. The three-dimensional cylindrical grid extents to $0 \leq x/D \leq 30$, $0 \leq r/D \leq 6$, with $(n_x, n_r, n_\theta) = (698, 136, 128)$, where n_x, n_r and n_θ are the number of points in the streamwise, radial and azimuthal direction, respectively. The database is sampled every delta $tc_\infty/D = 0.1$ acoustic time units, resulting in a cutoff (Nyquist) frequency of $St = \Delta f D/U_j = 3.33$. The jet operating conditions and simulation parameters are summarised in table 1.

In order to extract the coherence decay information, post-processing of the velocity data is required. The LES data is Fourier transformed in the azimuthal direction in order to extract the $m = 0$ axisymmetric mode. Prior to the temporal Fourier transform used to extract frequency-dependent information, a Hann window is used to divide the signal into data blocks of 178 time samples with 50% overlap.

Table 1 Jet Operating Conditions

Case	M_j	T_j/T_∞	M_a	Re	Sim. Duration	Sampling Period	Nyquist Freq.	Num. Snapshots
B118	1.5	1.0	1.5	3×10^5	215	0.1	3.33	5000

IV. Methodology & Theory

A. BBSAN Source Model

We adopt the previous nonlinear source description for BBSAN [1, 10, 15, 42] as shown in equation 2. The far-field sound is obtained using a convolution of the source CSD with the free-field Green's function (equation 6). By describing the source in such a manner, the turbulent fluctuations (u_t) and the modulations due to the shock-cells (u_s) are obtained independently. In order to construct the source term, we need to define both the axial and radial structure of u_s and u_t. We will only be studying the axisymmetric mode ($m = 0$) and hence a two-dimensional description of the source is sufficient. After arriving at the two-dimensional, axisymmetric description of the source term, it is integrated radially to

form an equivalent line source.

We educe the wavepacket behaviour from Brès et al. [2] high fidelity LES database of an ideally expanded $M_j = 1.5$ jet. The database has been validated and we use it to inform the wavepacket parameters (k_h, L_c) via results of linear PSE. Due to the slow-varying assumption of the base flow in the PSE formulation, we decided not to use a base flow with shocks but rather the ideally-expanded jet with the same perfectly-expanded jet velocity M_j. While this is consistent with the methodology of previous BBSAN studies [42], it is not possible to study the effects that the shock cells might have on the instability waves [49]. The two-point behaviour of the wavepacket is also probed from the azimuthally decomposed velocity field of the jet, allowing the CSD to be computed to recover the MSC.

The shock-cells are represented by zero-frequency eigenmodes of a locally parallel jet, modelled as a vortex sheet, as proposed by Pack & Prandtl, ensuring that the model remains grounded in stability theory. The fluctuations u_t and u_s are then combined to form the BBSAN source term. An overview of the method is shown in figure 1 and details of each u_s and u_t component are discussed in the following sections.

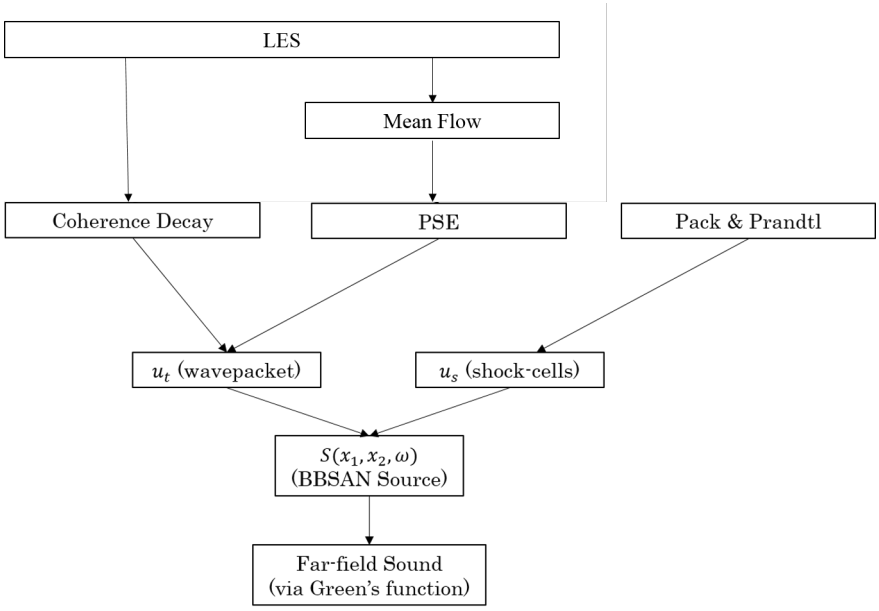

Fig. 1 Overview of the proposed methodology.

B. Pack & Prandtl Shock-cell Model

The shock-cell disturbances are treated as stationary waveguide modes of the jet flow as proposed by Prandtl [44], Pack [45], where the shear layer is modelled as a vortex sheet. For small disturbances, the linearised flow equations can be solved and the velocity fluctuations due to shock-cells u_s is given by

$$u_s(x, r) = \sum_n c_{s_n} \Phi(r) \frac{1}{2} \left\{ e^{\mathrm{i}k_{s_n} x} + e^{-\mathrm{i}k_{s_n} x} \right\}. \tag{9}$$

The radial profile $\Phi(r)$ is described by the Bessel functions of order 0 and 1. The shock-cell waveguide modes n are described by the wavenumbers k_{s_n} and the amplitude terms c_{s_n}. While the fundamental mode ($n = 1$) predicts the BBSAN peak frequency lobe well, higher-order shock-cell modes are required for frequencies greater than the peak and in the upstream direction [3, 42].

C. Parabolised Stability Equations

The wavepackets are based on linear stability theory. Since the jet mean flow is slowly diverging, we use parabolised stability equations (PSE) to describe the velocity fluctuations of the jet. PSE have been extensively used [40, 42, 50] to

model turbulent jets.

The flow quantities are first non-dimensionalised. Length quantities are normalised by the jet diameter D while velocities by the ambient speed of sound c_∞. Pressure p and temperature T are normalised by $\rho_\infty c_\infty^2$ and c_∞^2/c_p, where c_p is the heat capacity ratio for air [51]. Density ρ can be obtained via the perfect gas law and the Prandtl number is fixed at 0.7 for air. By working in cylindrical co-ordinates, the non-dimensionalised fluid properties of a jet can be described by the vector $\mathbf{q}$ and can be decomposed into a mean component $\bar{\mathbf{q}}(x, r)$ and a fluctuating component $\mathbf{q}'(x, r, \theta, t)$

$$\mathbf{q}(x, r, \theta, t) = \bar{\mathbf{q}}(x, r) + \mathbf{q}'(x, r, \theta, t). \tag{10}$$

The vector $\mathbf{q}$ refers to the dependent flow variables of interest, $\mathbf{q} = (u_x, u_r, u_\theta, T, \rho)$, where u_x, u_r and u_θ are the axial, radial and azimuthal velocity components respectively. The thermodynamic variables include T and ρ, which are the temperature the density of the fluid respectively. The problem is formulated in cylindrical coordinates. For stability calculations, an appropriate ansatz to model the velocity fluctuations for a compressible jet is given as

$$\mathbf{q}'(x, r, \theta, t) = \hat{\mathbf{q}}(x, r) e^{-\mathrm{i}\omega t} e^{\mathrm{i}m\theta}. \tag{11}$$

The term $\hat{\mathbf{q}}$ is the Fourier coefficient in space, m is the azimuthal wavenumber and $\omega = 2\pi St M_a$ is the angular frequency of the fluctuations. In the PSE framework, it is assumed that $q'(x, r, \theta, t)$ can be further decomposed into a slow and fast varying component. Hence, the appropriate multiple-scales ansatz as first proposed by Crighton and Gaster [52] can be written as

$$\mathbf{q}'(x, r, \theta, t) = \hat{\mathbf{q}}(x, r)) e^{\mathrm{i}\int \alpha(x')dx'} e^{-\mathrm{i}\omega t} e^{\mathrm{i}m\theta}, \tag{12}$$

where the slowly-varying part is described by the $\hat{\mathbf{q}}$ shape function and the fast part $e^{\mathrm{i}\int \alpha(x')dx'}$. The term $\alpha(x')$ is the complex-valued hydrodynamic wavenumber that varies with axial direction.

The ansatz as described in equation 12 can be substituted into the governing linearised equations where viscosity is not accounted for. The resultant matrix system can be recast into the following compact form (exact terms can be found in Gudmundsson and Colonius [30])

$$[\mathbf{A}(\bar{\mathbf{q}}, \alpha, \omega) + \mathbf{B}(\bar{\mathbf{q}})]\hat{\mathbf{q}} + \mathbf{C}(\bar{\mathbf{q}})\frac{\partial \hat{\mathbf{q}}}{\partial x} + +\mathbf{D}(\bar{\mathbf{q}})\frac{\partial \hat{\mathbf{q}}}{\partial x} = 0. \tag{13}$$

To find $\alpha_{m,\omega}(x)$ and $q(x, r)$, the system is discretised and solved by streamwise spatial marching. We used Chebyshev polynomials to discretise in the radial direction and first-order finite differences is used to approximate the axial derivatives. The axial step-size Δx is limited by the numerical stability condition as specified by Li and Malik [53]

$$\Delta x \geq \frac{1}{|Re\left\{\alpha_{m,\omega}(x)\right\}|}. \tag{14}$$

A complete description of the procedure is provided by Gudmundsson and Colonius [30] and a good summary is provided by Sasaki et al. [54]. To initiate the marching problem, initial flow conditions at the nozzle exit plane are provided by using the eigenfunction corresponding to the most dominant Kelvin-Helmholtz instability mode from solving the locally-parallel stability problem of the base flow which is the mean flow from the LES data.

In the pre-processing of the LES mean flow, no smoothing of the base flow was used, though analytical fits can be implemented to avoid non-smoothness problems [55]. The LES grid was interpolated onto the PSE grid via linear interpolation and for each frequency solved on its own axial grid given the condition specified in equation 14. The amplitude of the wavepackets is undefined since PSE is a linear problem and we have just multiplied it by a constant to match experimental data. A more rigorous approach, which we have not pursued for this study, will be to compute an alignment metric across a range of frequencies with experimental data [40, 56]. The $\alpha_{m,\omega}(x)$ and $q(x, r)$ terms are used to identify the k_h and L parameters for the wavepacket at a given frequency as shown in equation 8.

D. Coherence Decay

We model the two-point coherence using the same Gaussian envelope as Cavalieri and Agarwal [35] as shown in equation 5. The model is used to fit the computed magnitude square coherence (MSC) from the azimuthally decomposed Fourier transformed LES data. The CSD of streamwise velocities at two axial points, $\langle u_x(x_1, r, \omega) u_x^*(x_2, r, \omega)\rangle$, and their corresponding power spectral density (PSD), are used to compute the MSC $\gamma^2(x_1, x_2, \omega, m)$ as

$$\gamma^2(x_1, x_2, \omega, m) = \frac{|\langle \hat{u}_{\omega,m}(x_1)\hat{u}^*_{\omega,m}(x_2)\rangle|^2}{\langle|\hat{u}^*_{\omega}(x_1)|^2\rangle\langle|\hat{u}^*_{\omega}(x_2)|^2\rangle}. \tag{15}$$

Due to the axisymmetry of the jet, the MSC does not depend on θ [24]. The MSC is calculated for all axial separations for a given reference position. The fitted coherence model is then used in the sound-source model in equation 8.

V. Wavepacket Solutions from PSE

In this section, we present solutions from linear PSE for a $M_j = 1.5$ jet. Results shown below are for the axisymmetric mode ($m = 0$). The same PSE code has also been used in both subsonic [33] and supersonic [55] flows.

Figure 2 depicts the real parts of the pressure component of the PSE solution for a range of frequencies. The contour plots show features consistent with solutions from stability analysis of supersonic jets in the literature [40, 42]. The PSE solutions capture both the near-field fluctuations as well as the propagating acoustic far-field noise. The wavelength of the sound field matches those of the most energetic wavepacket; the wavepacket is 'acoustically matched' to the sound field that it radiates [17]. This condition is also seen in wavenumber space [35, 40] and the propagating sound waves are described by Tam [14] as Mach wave radiation. The wavepacket envelope shape is recovered. As frequency increases, the axial location of the wavepacket peak (x_0) shifts further upstream and the spatial wavelength decreases.

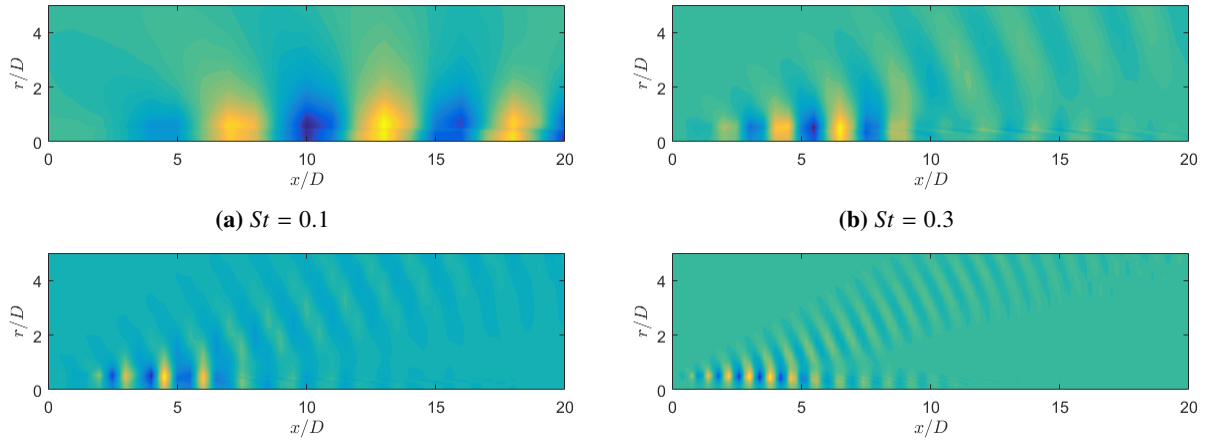

(a) $St = 0.1$ **(b)** $St = 0.3$

(c) $St = 0.5$ **(d)** $St = 0.9$

Fig. 2 Pressure component contour profiles from PSE solution for a $M_j = 1.5$ isothermal jet for a range of frequencies.

Radial profiles of PSE solutions are shown in figure 3. One can observe the phase shift between two sides of the mixing layer. This is consistent with the findings of Cavalieri et al. [50] and Ray and Lele [42] in subsonic jets.

Lastly, we show the power spectral density of the axial velocity fluctuations integrated radially for a range of frequencies in figure 4. The fluctuation energy of the axial velocity component forms the classical wavepacket envelope shape. The PSE results confirm the extended nature of wavepackets for lower-order azimuthal modes. While symmetric Gaussian functions have been used in previous studies to fit the PSD of the velocity fluctuations [35, 36], it can be seen from figure 4 that at higher frequencies the envelope has an asymmetric shape. Nevertheless, to be consistent with the current model, a symmetric Gaussian fit was used. Future attempts to model wavepacket PSD shapes should capture

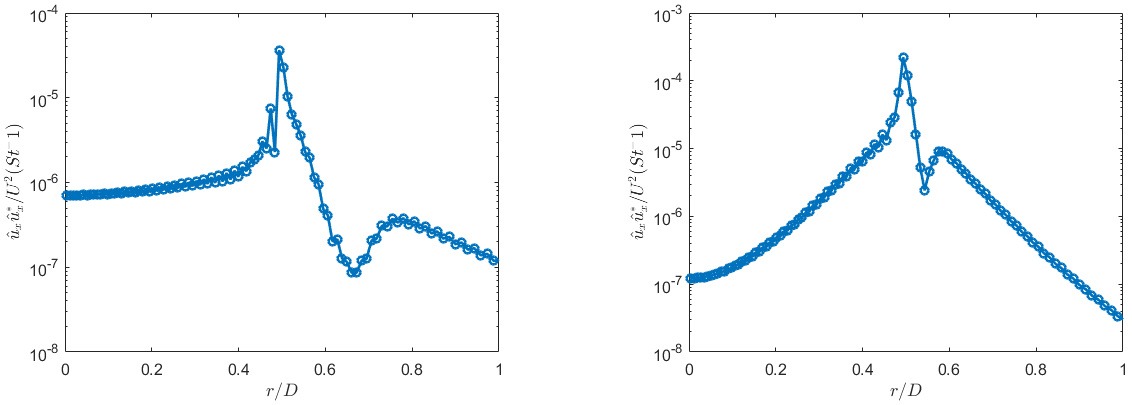

(a) $St = 0.3$ **(b)** $St = 0.9$

Fig. 3 Instability radial profiles for a $M_j = 1.5$ isothermal jet at axial station $x/D = 2.0$.

this asymmetry. Along with the real part of the complex wavenumber $\alpha_{m,\omega}(x)$ (results not shown here), we extracted the wavepacket wavenumber k_h and characteristic length L which form the turbulent fluctuation component u_t of the source term (equation 6).

VI. Large-Eddy Simulation Results

We compare the velocity fluctuations along the jet centerline between the LES data and the $m = 0$ mode solution of the PSE in figure 5. The PSE solutions have been multiplied by a constant to match the magnitudes from the LES data.

Figure 5 shows an increase in fluctuation energy of approximately four orders of magnitude. This is also observed in hot wire measurements in subsonic jets [50]. Within the potential core of the jet ($x/D \leq 6$), the maximum fluctuation energy ranges from $10^{-8} - 10^{-4}$, which is an order of magnitude smaller ($10^{-4} - 10^{-3}$) than those found by Cavalieri et al. [50] of a subsonic $M = 0.4$ jet. This is consistent with the notion that the growth rates of the instabilities are suppressed as Mach number increases due to compressiblity effects.

We note that in figure 5, while the PSE solutions are able to capture the increase in fluctuation energy in regions close to the nozzle exit, the LES PSD data increases more rapidly for the region $x/D \leq 2$. At positions further downstream, the LES data diverges from the PSE solution. This divergence is consistent with previous work by Suzuki and Colonius [27], Gudmundsson and Colonius [30] and Cavalieri et al. [50]. It is attributed to wavepacket growth via non-modal mechanisms caused by non-linear forcing [57].

VII. Coherence Decay Length

The coherence decay length of the azimuthally decomposed $m = 0$ instability wave, while previously modelled [35, 36], had only been previously measured experimentally by Jaunet et al. [24] via twin synchronised time-resolved stereo PIV systems. The coherence lengths were obtained by computing the MSC between two points in the flow. To capture coherence decay, Jaunet et. al measured it at a fixed axial location of $x/D = 3.0$ and a radial position of $r/D = 0.42$. In this present study, however, we have chosen to have the reference position x_0 where the wavepacket peaks and the fixed radial position of $r/D = 0.5$. Jaunet et al. [24] did show that difference in coherence decay behaviour between the two radial positions remain minimal.

While we find that the coherence decay function is asymmetric [24, 39] and an improved fit can be obtained by using a two-sided convolution of a Gaussian and exponential [39, 58], a simple Gaussian function was used to model coherence decay (equation 5). This is consistent with the proposed source model in equation 2 and will allow a comparison between the present findings with the constant coherence length used by Wong et al. [1].

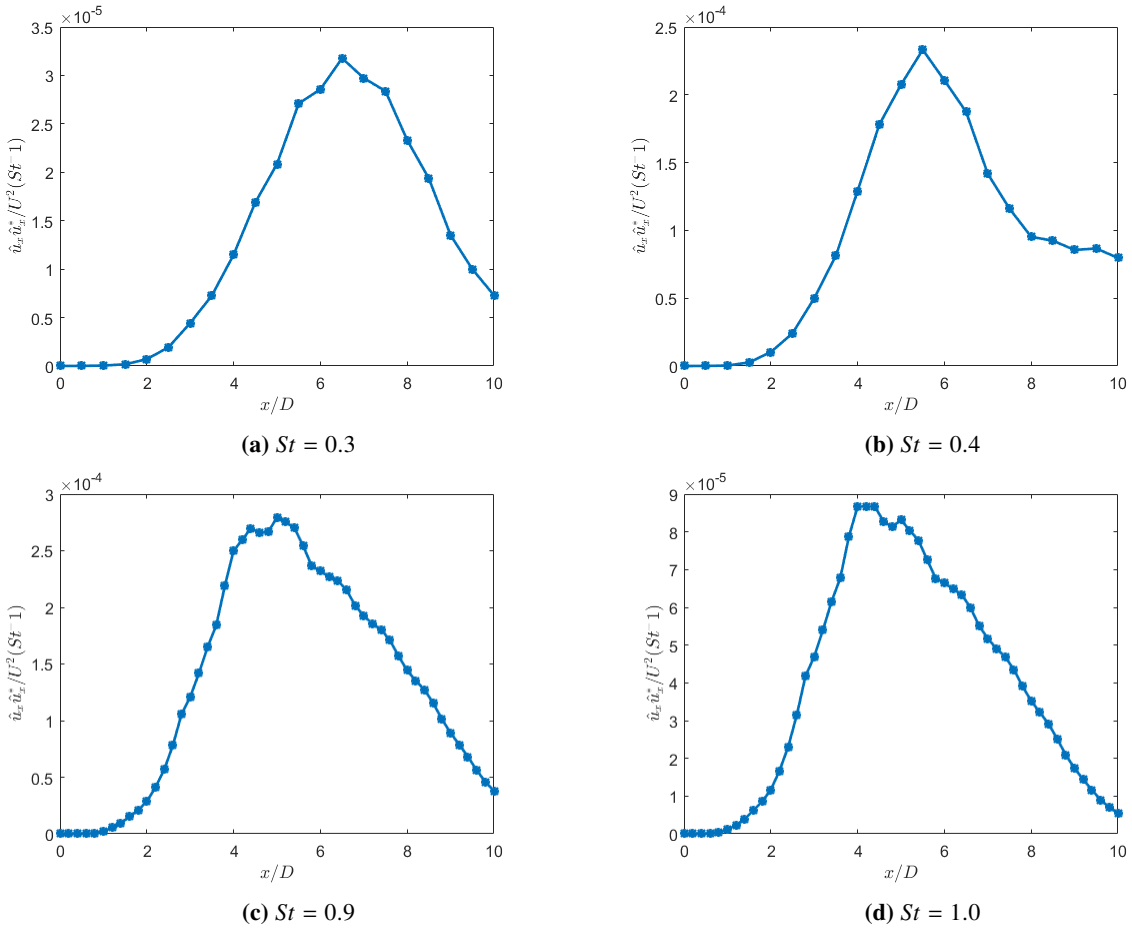

(a) $St = 0.3$ **(b)** $St = 0.4$

(c) $St = 0.9$ **(d)** $St = 1.0$

Fig. 4 PSE solutions of the integrated PSD of the axial velocity fluctuations u_x for a $M_j = 1.5$ isothermal jet.

The one-sided MSC is shown in figure 6 showing a clear decay as a function of downstream axial separation distance. Moreover, the decay rate is a function of frequency, with a quicker decay rate as frequency increases. By fitting the MSC with a Gaussian function, the characteristic length scale L_c in equation 15 can be obtained. The frequency dependence of L_c can be seen in figure 7 and shows that the ad-hoc assumption of the constant coherence length used by Wong et al. [1] of $1.0D$ is not realistic. It should be noted that compared to the subsonic $M = 0.4$ jet [24, 39], the coherence lengths obtained for the current supersonic jet $M_j = 1.5$ are much smaller. This suggests that wavepackets in supersonic jets desynchronise over a shorter distance compared to its subsonic counter part. The coherence length trend seen in figure 7 is similar to the decay in the 'cross-coherence' of the sources found by Lele [15].

VIII. Far-field BBSAN Sound Prediction

By using the source description in equation 2 and combining the Pack & Prandtl shock-cell model with the outputs from the PSE analysis and LES database, we can obtain a two-dimensional source description for BBSAN. To aide the analysis, solutions from PSE and the MSC results have been smoothed by fitting the appropriate analytical functions as shown in equation 2. Similar to Wong et al. [1], a total of ten ($n = 10$) shock-cell modes have been used. The far-field sound behaviour can be obtained by using the appropriate free-field Green's function. The line source integration region extends from $0 \leq x/D \leq 20D$ corresponding to 1000 grid points. A Hann-windowing technique is used in order to make the downstream source amplitude decay to remove artificial errors from an abrupt discontinuity of the source [59].

Figure 8 shows the comparison between model predictions and experimental data from NASA's Small Hot Jet acoustic Rig (SHJAR) for a supersonic jet operating at $M_j = 1.5$ and $M_d = 1.0$ at three observer angles (80^o, 90^o and 130^o) relative to the downstream jet axis [18]. The degree of underexpansion, captured by the off-design parameter

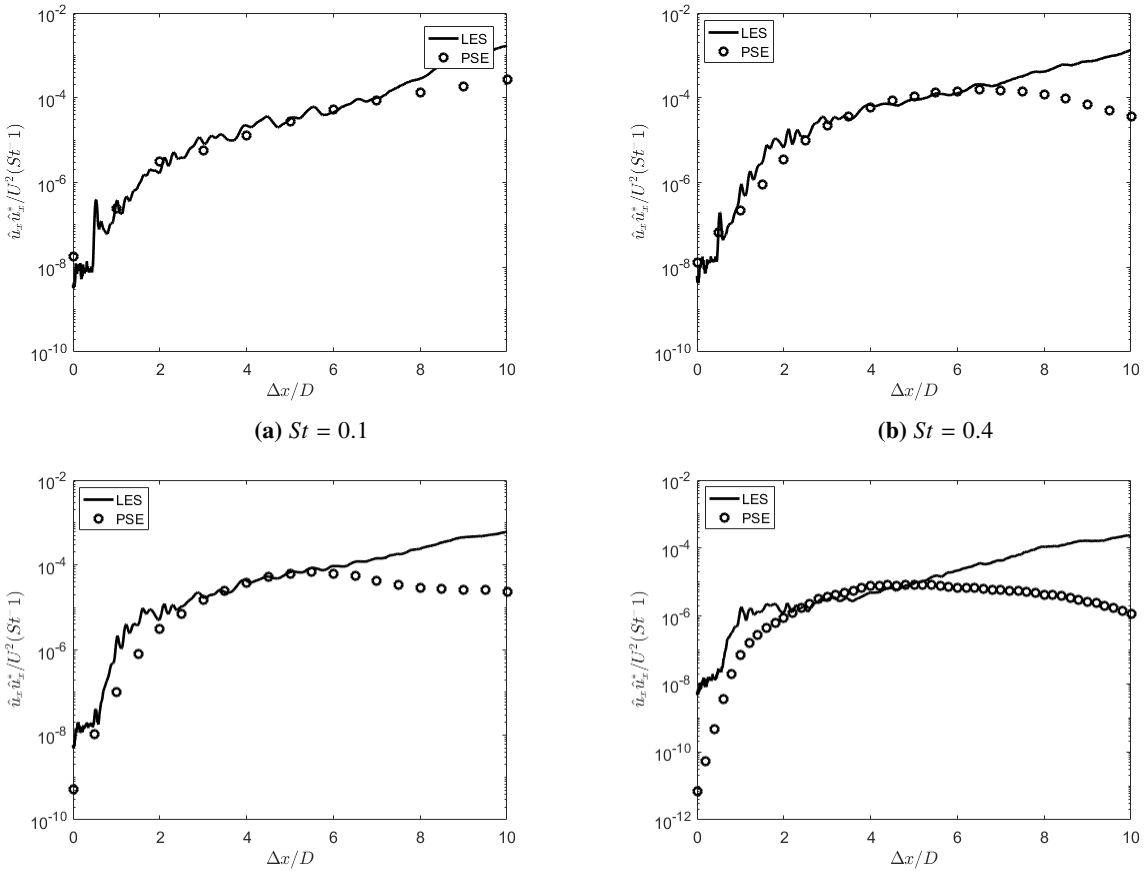

(a) $St = 0.1$ **(b)** $St = 0.4$

(c) $St = 0.5$ **(d)** $St = 0.9$

Fig. 5 Comparison between PSE solutions and LES PSD of velocity fluctuations u_x along the jet centerline for a $M_j = 1.5$ isothermal jet.

$\beta = \sqrt{M_j^2 - M_d^2}$, is matched. The observer location is located at $R = 100D$. The peak maximum amplitudes are matched by scaling it with a constant factor. There is a fair agreement between the two models. As the angle to the jet downstream axis increases, the movement of the BBSAN peak to lower Strouhal numbers is reproduced. The agreement in the roll-off at low frequencies is well captured at all angles. However, there is a small under-prediction of the peak frequency at 80^o. Moreover, the predictions begin to diverge at higher Strouhal frequencies ($St \geq 1$). Below $St = 0.2 - 0.3$, the dominance of turbulent mixing noise rather than BBSAN at low frequencies results in an underprediction in SPL, which is expected.

When compared to the far-field noise prediction of Wong et al. [1] (dashed lines in figure 8), the importance of capturing the correct coherence length is seen in the shape of the predicted peak. The suppression of higher-order peaks is evident in both cases with the inclusion of coherence decay. Wong et al. [1] used a constant coherence length to establish the impact of coherence decay but obtained an overprediction at low frequencies. Contrastingly, using a coherence length with frequency dependence was found to obtain the correct low frequency roll-off as observed in figure 8. The current results further confirm the importance of coherence decay in supersonic shock-containing flows as found by [1].

Nevertheless, there remain differences between the current predictive model and those from literature and experiments. The underprediction of high frequency sound could be due to the incorrect scaling of the free amplitude of the linear PSE solution. By projecting the leading mode from SPOD of LES data onto the PSE solutions, Antonialli et al. [56] found an exponential dependence of wavepacket amplitude with Strouhal. No such dependence has been implemented

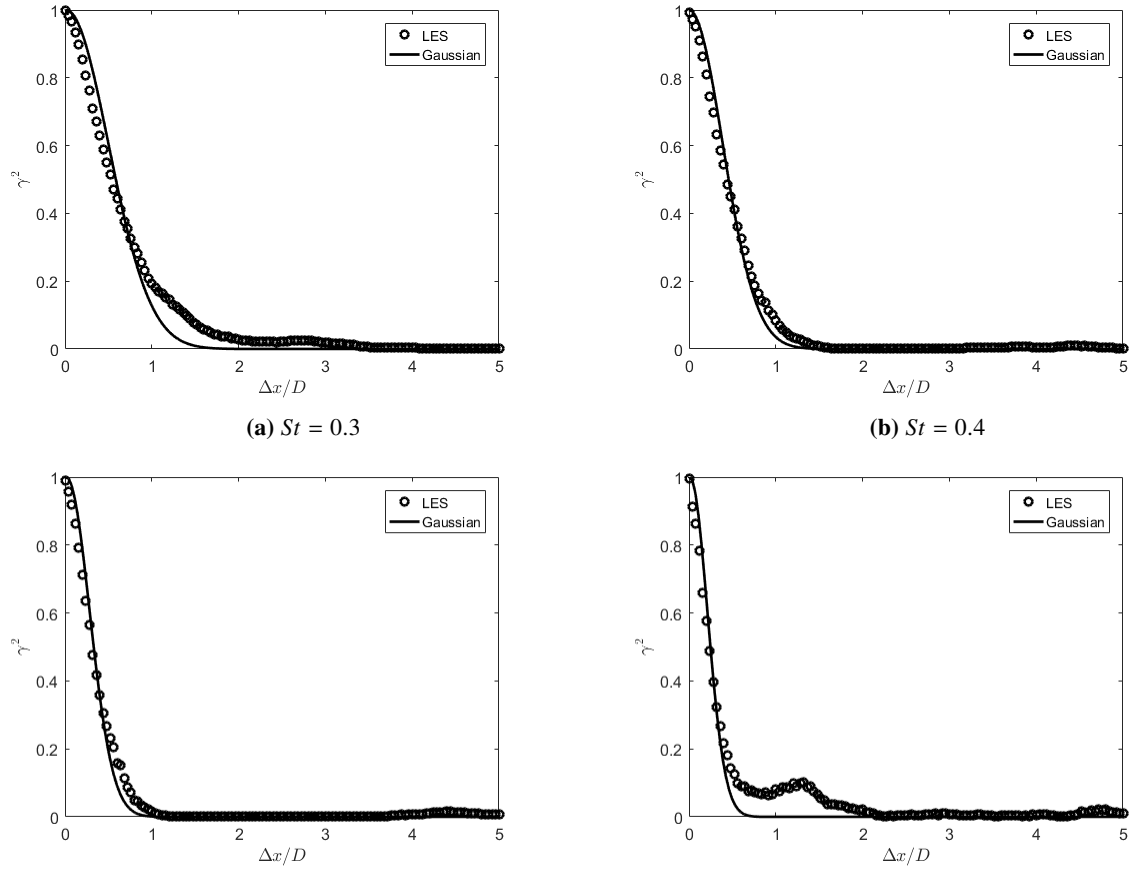

(a) $St = 0.3$ **(b)** $St = 0.4$

(c) $St = 0.9$ **(d)** $St = 1.0$

Fig. 6 Magnitude-squared coherence function (MSC) as a function of axial separation distance Δx for the $m = 0$ mode. Reference axial position x_0 is the peak of the wavepacket and radial position at $r/D = 0.5$.

in the current results. The negligence of higher-order azimuthal wavepacket modes [60] could have also affected sound prediction at upstream angles. Moreover, there remains an underprediction in the peak Strouhal frequency at low downstream angles (80^o). This was also observed in the previous analytical model of Wong et al. [1]. This could be due to the increase in interference of the line source at downstream directions for extended sources Cavalieri et al. [20], though further investigation is required.

IX. Conclusion

Motivated by the results of the two-point BBSAN source model developed by Wong et al. [3], flow properties based on stability theory were obtained as inputs into the model. The LES data of a $M_j = 1.5$ ideally-expanded supersonic turbulent jet [2] was used as the base flow for obtaining the linear PSE solutions of the flow. The 'jittering' non-linear behaviour of the flow was modelled as coherence decay between two points of the jet and the relevant length scale was extracted.

The PSE solutions at different frequencies are presented and the average wavepacket characteristics were obtained including its spatial envelope size and wavenumber. The radial structure and growth in the initial region close to the nozzle exit have similar behaviour to wavepackets in subsonic jets [39, 50]. The coherence decay length scale was found to be much shorter than its subsonic counterpart.

Using the results from the LES and PSE solutions, coupled with the Pack & Prandtl representation of the shock cells,

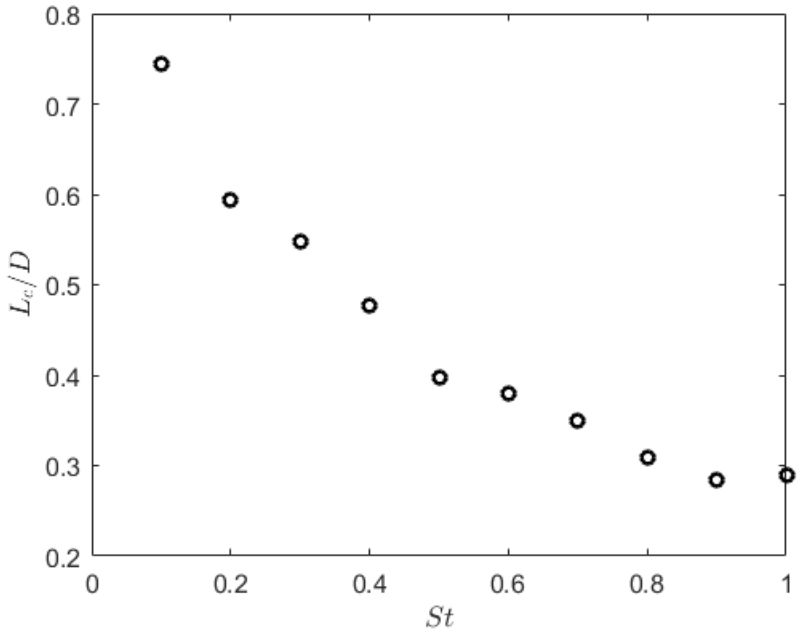

Fig. 7 Normalised coherence length as a function of Strouhal number. Reference position x_0 is the peak of the wavepacket.

far-field BBSAN spectra are presented for multiple radiation angles. The far-field predictions re-affirm the importance of coherence decay in supersonic shock-containing flows. The higher-order peaks are suppressed and a frequency dependant length scale improved the low-frequency roll-off of the BBSAN peak compared to the predictions made by Wong et al. [1].

Future works will focus on refining the methodology, which includes using appropriate analytical functions to fit the data. An analytical fit to the LES mean flow should be used to avoid non-smoothness problems [55] as well as new non-Gaussian functions to fit the asymmetric behaviour of the wavepacket envelope and the magnitude square coherence of the jet [39]. In order to improve noise predictions at higher frequencies, a more rigorous scaling of the free-amplitude PSE solutions is required. These refinements should improve the current BBSAN predictions and provide a better indication of the robustness of the current model.

Acknowledgements

This work was supported by the Australian Government via a Research Training Program (RTP) Scholarship and the Endeavour Leadership Program (ELP). The project is also funded by the Australian Research Council through the Discovery Projects scheme. The authors would like to thank Dr. Guillaume Brès at Cascade Technologies for providing the simulation database. The LES work was supported by ONR, with computational resources provided by DoD HPCMP. M.H.W would also like to thank Mr. I. Maia and Ms. R. Kirby for their insightful advice and recommendations.

References

[1] Wong, M. H., Jordan, P., Honnery, D. R., and Edgington-Mitchell, D., "Impact of coherence decay on wavepacket models for broadband shock-associated noise in supersonic jets," *Journal of Fluid Mechanics*, Vol. 863, 2019, pp. 969–993.

[2] Brès, G., Ham, F., Nichols, J., and Lele, S., "Unstructured large-eddy simulations of supersonic jets," *AIAA Journal*, 2017, pp. 1164–1184.

[3] Wong, M. H., Edgington-Mitchell, D. M., Honnery, D. R., Jordan, P., and Savarese, A., "Kinematic wavepacket model for

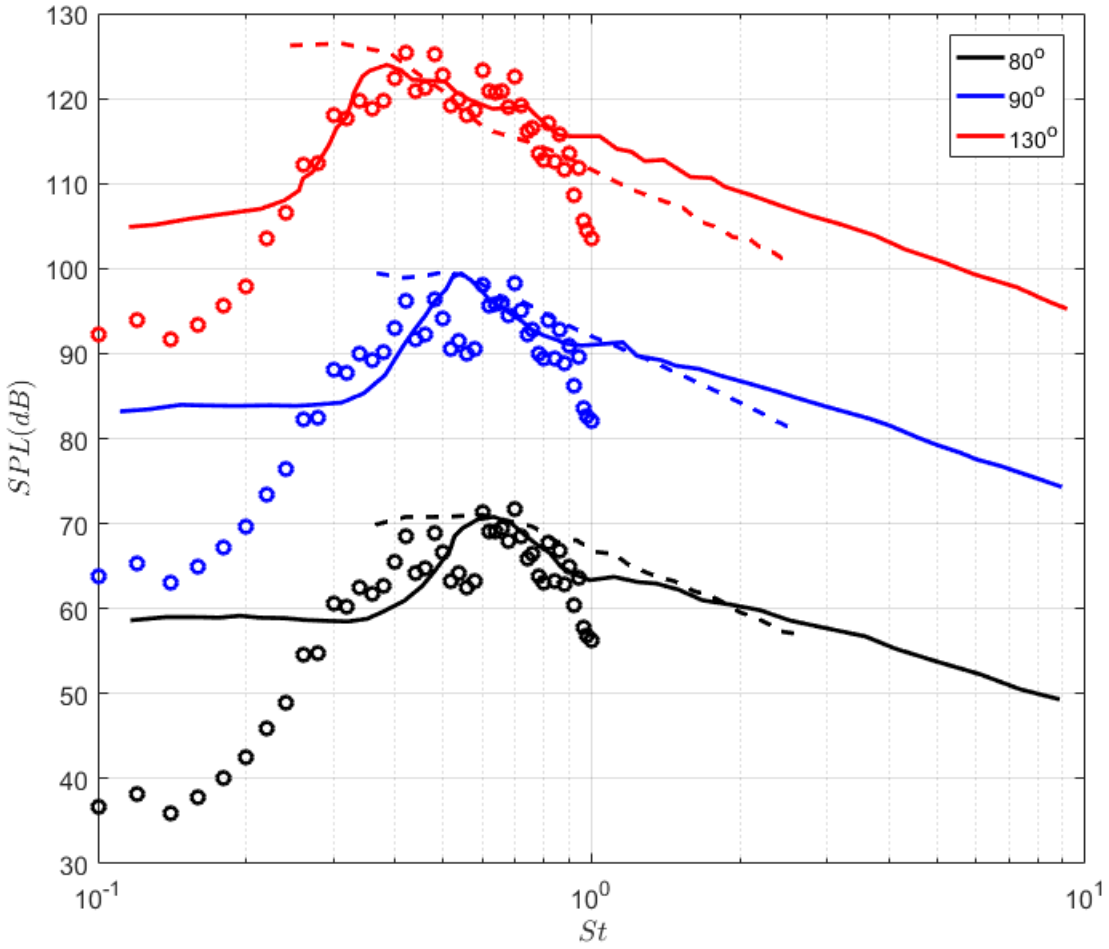

Fig. 8 Comparison of far-field sound pressure level (arbitrary) as a function of frequency at 80^o (black), 90^o (blue) and 130^o (red) observation angles. 'o' represent predicted spectrum from model, '- -' is obtained from Wong et al. [1] BBSAN model and '-' from NASA experimental data.

broadband shock associated noise in underexpanded supersonic jets," *2018 AIAA/CEAS Aeroacoustics Conference*, 2018, p. 3465.

[4] Tam, C., "Broadband shock-associated noise of moderately imperfectly expanded supersonic jets," *Journal of Sound and Vibration*, Vol. 140, No. 1, 1990, pp. 55–71.

[5] Lighthill, M., "On sound generated aerodynamically. I. General theory," *Proceedings of the Royal Society of London A: Mathematical, Physical and Engineering Sciences*, Vol. 211, The Royal Society, 1952, pp. 564–587.

[6] Edgington-Mitchell, D., Oberleithner, K., Honnery, D., and Soria, J., "Coherent structure and sound production in the helical mode of a screeching axisymmetric jet," *Journal of Fluid Mechanics*, Vol. 748, 2014, pp. 822–847.

[7] Raman, G., "Supersonic jet screech: half-century from Powell to the present," *Journal of Sound and Vibration*, Vol. 225, No. 3, 1999, pp. 543–571.

[8] Vaughn, A. B., Neilsen, T. B., Gee, K. L., Wall, A. T., Micah Downing, J., and James, M. M., "Broadband shock-associated noise from a high-performance military aircraft," *The Journal of the Acoustical Society of America*, Vol. 144, No. 3, 2018, pp. EL242–EL247.

[9] Harper-Bourne, M., and Fisher, M., "The noise from shock waves in supersonic jets," *AGARD-CP-131*, Vol. 11, 1973, pp. 1–13.

[10] Tam, C., Seiner, J., and Yu, J., "Proposed relationship between broadband shock associated noise and screech tones," *Journal of sound and vibration*, Vol. 110, No. 2, 1986, pp. 309–321.

[11] Morris, P., and Zaman, K., "Velocity measurements in jets with application to noise source modeling," *Journal of sound and vibration*, Vol. 329, No. 4, 2010, pp. 394–414.

[12] Kalyan, A., and Karabasov, S., "Broad band shock associated noise predictions in axisymmetric and asymmetric jets using an improved turbulence scale model," *Journal of Sound and Vibration*, Vol. 394, 2017, pp. 392–417.

[13] Tan, D., Kalyan, A., Gryazev, V., Wong, M., Honnery, D., Edgington-Mitchell, D., and Karabasov, S., "On the Application of Shock-Associated Noise Models to PIV Measurements of Screeching Axisymmetric Cold Jets," *23rd AIAA/CEAS Aeroacoustics Conference*, 2017, p. 3028.

[14] Tam, C., "Supersonic jet noise," *Annual Review of Fluid Mechanics*, Vol. 27, No. 1, 1995, pp. 17–43.

[15] Lele, S., "Phased array models of shock-cell noise sources," *AIAA Paper*, Vol. 2841, 2005, p. 2005.

[16] Lighthill, M., "On sound generated aerodynamically. I. General theory," *Proceedings of the Royal Society of London A: Mathematical, Physical and Engineering Sciences*, Vol. 211, The Royal Society, 1952, pp. 564–587.

[17] Crighton, D., "Basic principles of aerodynamic noise generation," *Progress in Aerospace Sciences*, Vol. 16, No. 1, 1975, pp. 31–96.

[18] Morris, P., and Miller, S., "Prediction of broadband shock-associated noise using Reynolds-averaged Navier-Stokes computational fluid dynamics," *AIAA journal*, Vol. 48, No. 12, 2010, p. 2931.

[19] Jordan, P., and Colonius, T., "Wave packets and turbulent jet noise," *Annual Review of Fluid Mechanics*, Vol. 45, 2013, pp. 173–195.

[20] Cavalieri, A. V., Jordan, P., and Lesshafft, L., "Wave-packet models for jet dynamics and sound radiation," *Applied Mechanics Reviews*, Vol. 71, No. 2, 2019, p. 020802.

[21] Mollo-Christensen, E., "Jet noise and shear flow instability seen from an experimenter's viewpoint," *Journal of Applied Mechanics*, Vol. 34, No. 1, 1967, pp. 1–7.

[22] Crow, S., and Champagne, F., "Orderly structure in jet turbulence," *Journal of Fluid Mechanics*, Vol. 48, No. 3, 1971, pp. 547–591.

[23] Michalke, A., "A wave model for sound generation in circular jets," 1970.

[24] Jaunet, V., Jordan, P., and Cavalieri, A., "Two-point coherence of wave packets in turbulent jets," *Physical Review Fluids*, Vol. 2, No. 2, 2017, p. 024604.

[25] Schmidt, O. T., Towne, A., Rigas, G., Colonius, T., and Brès, G. A., "Spectral analysis of jet turbulence," *Journal of Fluid Mechanics*, Vol. 855, 2018, pp. 953–982.

[26] Cavalieri, A., Jordan, P., Colonius, T., and Gervais, Y., "Axisymmetric superdirectivity in subsonic jets," *Journal of fluid Mechanics*, Vol. 704, 2012, pp. 388–420.

[27] Suzuki, T., and Colonius, T., "Instability waves in a subsonic round jet detected using a near-field phased microphone array," *Journal of Fluid Mechanics*, Vol. 565, 2006, pp. 197–226.

[28] Breakey, D., Jordan, P., Cavalieri, A., and Léon, O., "Near-field wavepackets and the far-field sound of a subsonic jet," *19th AIAA/CEAS aeroacoustics conference*, 2013, p. 2083.

[29] Tinney, C., and Jordan, P., "The near pressure field of co-axial subsonic jets," *Journal of Fluid Mechanics*, Vol. 611, 2008, pp. 175–204.

[30] Gudmundsson, K., and Colonius, T., "Instability wave models for the near-field fluctuations of turbulent jets," *Journal of Fluid Mechanics*, Vol. 689, 2011, pp. 97–128.

[31] Cavalieri, A., Jordan, P., Wolf, W., and Gervais, Y., "Scattering of wavepackets by a flat plate in the vicinity of a turbulent jet," *Journal of sound and Vibration*, Vol. 333, No. 24, 2014, pp. 6516–6531.

[32] Lesshafft, L., Semeraro, O., Jaunet, V., Cavalieri, A. V., and Jordan, P., "Resolvent-based modelling of coherent wavepackets in a turbulent jet," *arXiv preprint arXiv:1810.09340*, 2018.

[33] Sasaki, K., Cavalieri, A., Jordan, P., Schmidt, O., Colonius, T., and Brès, G., "High-frequency wavepackets in turbulent jets," *Journal of Fluid Mechanics*, Vol. 830, 2017.

[34] Piantanida, S., Jaunet, V., Huber, J., Wolf, W. R., Jordan, P., and Cavalieri, A. V., "Scattering of turbulent-jet wavepackets by a swept trailing edge," *The Journal of the Acoustical Society of America*, Vol. 140, No. 6, 2016, pp. 4350–4359.

[35] Cavalieri, A., and Agarwal, A., "Coherence decay and its impact on sound radiation by wavepackets," *Journal of Fluid Mechanics*, Vol. 748, 2014, pp. 399–415.

[36] Baqui, Y., Agarwal, A., Cavalieri, A., and Sinayoko, S., "A coherence-matched linear source mechanism for subsonic jet noise," *Journal of Fluid Mechanics*, Vol. 776, 2015, pp. 235–267.

[37] Zhang, M., Jordan, P., Lehnasch, G., Cavalieri, A., and Agarwal, A., "Just enough jitter for jet noise?" *20th AIAA/CEAS Aeroacoustics Conference*, 2014, p. 3061.

[38] Cavalieri, A., Jordan, P., Agarwal, A., and Gervais, Y., "Jittering wave-packet models for subsonic jet noise," *Journal of Sound and Vibration*, Vol. 330, No. 18, 2011, pp. 4474–4492.

[39] Maia, I., Jordan, P., Jaunet, V., and Cavalieri, A., "Two-point wavepacket modelling of jet noise," *23rd AIAA/CEAS Aeroacoustics Conference*, 2017, p. 3380.

[40] Sinha, A., Rodríguez, D., Brès, G., and Colonius, T., "Wavepacket models for supersonic jet noise," *Journal of Fluid Mechanics*, Vol. 742, 2014, pp. 71–95.

[41] Suzuki, T., "Wave-Packet Representation of Shock-Cell Noise for a Single Round Jet," *AIAA Journal*, 2016.

[42] Ray, P., and Lele, S., "Sound generated by instability wave/shock-cell interaction in supersonic jets," *Journal of fluid mechanics*, Vol. 587, 2007, pp. 173–215.

[43] Tan, D., Honnery, D., Kalyan, A., Gryazev, V., Karabasov, S., and Edgington-Mitchell, D., "Equivalent shock-associated noise source reconstruction of screeching underexpanded unheated round jets," *AIAA Journal*, Vol. 57, No. 3, 2018, pp. 1200–1214.

[44] Prandtl, L., *Über die stationären Wellen in einem Gasstrahl*, Hirzel, 1904.

[45] Pack, D., "A note on Prandtl's formula for the wave-length of a supersonic gas jet," *The Quarterly Journal of Mechanics and Applied Mathematics*, Vol. 3, No. 2, 1950, pp. 173–181.

[46] Brès, G., Nichols, J., Lele, S., and Ham, F., "Towards best practices for jet noise predictions with unstructured large eddy simulations," *42nd AIAA Fluid Dynamics Conference and Exhibit*, 2012, p. 2965.

[47] Schlinker, R., Simonich, J., Shannon, D., Reba, R., Colonius, T., Gudmundsson, K., and Ladeinde, F., "Supersonic jet noise from round and chevron nozzles: experimental studies," *15th AIAA/CEAS Aeroacoustics Conference (30th AIAA Aeroacoustics Conference)*, 2009, p. 3257.

[48] Brès, G. A., Jordan, P., Jaunet, V., Le Rallic, M., Cavalieri, A. V., Towne, A., Lele, S. K., Colonius, T., and Schmidt, O. T., "Importance of the nozzle-exit boundary-layer state in subsonic turbulent jets," *Journal of Fluid Mechanics*, Vol. 851, 2018, pp. 83–124.

[49] Ansaldi, T., Airiau, C., Pérez Arroyo, C., and Puigt, G., "PSE-based sensitivity analysis of turbulent and supersonic single stream jet," *22nd AIAA/CEAS Aeroacoustics Conference*, 2016, p. 3052.

[50] Cavalieri, A., Rodríguez, D., Jordan, P., Colonius, T., and Gervais, Y., "Wavepackets in the velocity field of turbulent jets," *Journal of fluid mechanics*, Vol. 730, 2013, pp. 559–592.

[51] AERONÁUTICA, M. P. E. E., and SASAKI, K., "ESTUDO E CONTROLE DE PACOTES DE ONDA EM JATOS UTILIZANDO AS EQUAÇÕES DE ESTABILIDADE PARABOLIZADAS," 2014.

[52] Crighton, D., and Gaster, M., "Stability of slowly diverging jet flow," *Journal of Fluid Mechanics*, Vol. 77, No. 2, 1976, pp. 397–413.

[53] Li, F., and Malik, M. R., "Spectral analysis of parabolized stability equations," *Computers & fluids*, Vol. 26, No. 3, 1997, pp. 279–297.

[54] Sasaki, K., Piantanida, S., Cavalieri, A., and Jordan, P., "Real-time modelling of wavepackets in turbulent jets," *Journal of Fluid Mechanics*, Vol. 821, 2017, pp. 458–481.

[55] Kleine, V. G., Sasaki, K., Cavalieri, A. V., Brès, G. A., and Colonius, T., "Evaluation of PSE as a model for supersonic jet using transfer functions," *23rd AIAA/CEAS Aeroacoustics Conference*, 2017, p. 4194.

[56] Antonialli, L., Cavalieri, A., Schmidt, O., Colonius, T., Jordan, P., Towne, A., Brés, G., , and Agarwal, A., "Amplitude scaling of turbulent-jet wavepackets," *23rd AIAA/CEAS Aeroacoustics Conference*, 2018, p. under review.

[57] Jordan, P., Zhang, M., Lehnasch, G., and Cavalieri, A. V., "Modal and non-modal linear wavepacket dynamics in turbulent jets," *23rd AIAA/CEAS Aeroacoustics Conference*, 2017, p. 3379.

[58] Jordan, P., Wells, R., Gervais, Y., and Delville, J., "Optimisation of correlation function models for statistical aeroacoustic noise prediction," *CFA/DAGA 2004 Acoustics conference, Strasbourg*, 2004.

[59] Martínez-Lera, P., and Schram, C., "Correction techniques for the truncation of the source field in acoustic analogies," *The Journal of the Acoustical Society of America*, Vol. 124, No. 6, 2008, pp. 3421–3429.

[60] Arroyo, C. P., and Moreau, S., "Azimuthal mode analysis of broadband shock-associated noise in an under-expanded axisymmetric jet," *Journal of Sound and Vibration*, Vol. 449, 2019, pp. 64–83.